A novel high entropy CoFeCrNiCu alloy filler to braze SiC ceramics

Gang Wang [a*], Yunlong Yang [a], Rujie He [b*], Caiwang Tan [c], Marko Huttula [d], Wei Cao [d, a]

[a] Anhui Key Laboratory of High-performance Non-ferrous Metal Materials, Anhui Polytechnic University, Wuhu 241000, PR China

[b] Institute of Advanced Structure Technology, Beijing Institute of Technology, Beijing 100081, PR China

[c] State Key Laboratory of Advanced Welding and Joining, Harbin Institute of Technology, Harbin 150001, PR China

[d] Nano and Molecular Systems Research Unit, University of Oulu, P.O. Box 3000, FIN-90014, Oulu, Finland

---

Corresponding authors: Gang Wang, Rujie He

E-mail addresses: gangwang@ahpu.edu.cn (G. Wang)*, herujie@bit.edu.cn (R. He)*

Abstract

In order to reduce intermetallic compound formations in brazed joints, a CoFeCrNiCu high entropy alloy was invented and employed to braze SiC ceramics. Results show that SiC ceramics were tightly and strongly brazed with the CoFeCrNiCu filler. Microstructure, phase and shear strength were systematically studied for joints brazed at different temperature. Main compositions were identified as high-entropy FCC, Cu(s, s), Si(s, s), and $Cr_{23}C_6$ phases, regardless the brazing temperature differences. After being brazed at 1453 K, the joint reached a maximum shear strength of 60 MPa, much higher than those brazed with conventional AgCuTi filler. Thanks to high entropy effect of the filler, random solid solution turned out in the seam and benefitted joint quality. The successful use of the CoFeCrNiCu high entropy alloy as a filler can expand application ranges of high entropy alloys and provide a new filler system to braze ceramics.

Keywords

SiC ceramic; high entropy alloy; brazing; microstructure; shear strength

1. Introduction

SiC ceramic has been widely applied in nuclear powerplants, semiconductors and machinery due to its outstanding high strength, high hardness, low density, good oxidation resistance, and low coefficient of thermal expansion [1-5]. However, its intrinsic properties of high hardness, brittleness, and low electrical conductivity hinder its formations in large sizes and complex shapes [6]. To extend the SiC application scope, various techniques have been assessed to join the ceramic to other metals and compounds [7-9]. Among them, the brazing technology is a simple, convenient and economical connection method and considered promising to solve problems arisen from the physical properties of the carbide.

Choosing a proper filler is important for brazing [10]. Conventionally, Ag-Cu-Ti-based fillers and Ni-based fillers are used in ceramics brazing [11]. It was found that addition of Zr element in the Ti-Ni eutectic filler facilitated SiC ceramics brazing. The shear strength of the joints was improved from 69 MPa to 112 MPa and a large amount of brittle intermetallic compound Ti_2Ni was generated in the joint [12]. The Ag-Cu-Ti composite filler was also modified with B_4C. Due to the presence of the B_4C, TiB whiskers and TiC particles were simultaneously formed in the Ag-based and Cu-based solid solutions. While a high shear strength of 140 MPa was reached, a large number of brittle TiCu phases turned out in the joint [13]. Zhong *et al.* studied microstructure and mechanical strength of SiC joints brazed with a Cr_3C_2-particles reinforced Ag-Cu-Ti filler. The carbide at an appropriate proportion in the filler became randomly distributed particulates in the brazed matrix. As a result, the Ag-rich

and Cu-rich solid solution phases were refined. However, the Cu_2Ti intermetallic phase was also associated with the solid solution formations [14]. From the above reports, while the Ni-based fillers and Ag-Cu-Ti-based fillers are good at introducing wetting effect on the ceramic surface, a large amount of brittle intermetallic compounds stayed at the brazed joints and deteriorated joint qualities due to large negative mixing enthalpies between Cu/Ni and Ti. Consequentially, Cu or Ni can easily react with Ti to reduce the activity of the Ti element and ruin joint performance. In addition, the expensive AgCuTi fillers are easily oxidized and rather soft. The low melting points of brazed products from the AgCu fillers damage the overall stabilities of the composites in high temperature. As a result, the application range of the joint SiC is limited [12]. Therefore, it is urgent to design a new type of filler for reliable self-joining of the SiC ceramic.

As a new kind of alloys, the high-entropy alloy has attracted great attention due to its high mechanical properties, and especially the good thermal stability at high temperature. In high-entropy alloy, component elements prefer random distributions instead of being alloyed intermetallically. The activity of each element is kept, and solid solutions are formed as the products after high temperature treatments [15]. In addition, slow diffusions of these component elements inhibit excessive dissolution of the base material into the brazing seam during the brazing process. Up to date, many high entropy alloys have been developed such as FeCrMnNiCo, AlCoCrFeNiTi, CoCrCuFeNiTi etc [16, 17]. However, application of high-entropy alloys has been scarcely reported in brazing. Zhang *et al.* successfully joined ZrB_2-SiC-C ceramic to

GH 99 superalloy by using a Ti/FeCoNiCrCu composite filler. Therein, the activities of Ti and Cr were preserved while the solid solution phase was formed in the brazing seam eventually. The (TiB + Cr-B)/solid solution was well bonded to ZSC and GH99. A maximum shear strength of 71 MPa was achieved [18]. The Ni-Mn-Fe-Co-Cu high entropy alloy brought in superior mechanical performances when employed to braze metals to Inconel 718. The maximum bending strength reached 140 MPa [19].

In this work, a high entropy alloy of CoFeCrNiCu alloy was prepared and employed as the brazing filler, owing to its simple solid solution structure, low melting point and common elements [20, 21]. Comprehensive studies of brazing temperature influences on interfacial structure and joint strength were carried out. The relation between the microstructural evolution and mechanical properties of the joints was assessed. It is found that an active interfacial reaction was reached between SiC and the active element of Cr during the brazing. Solid-solution bulks were formed as the matrices at the brazing seams, leading to mechanical enhancements of the joints. Moreover, a formation mechanism of brazed joint was proposed based on element diffusion schemes.

2. Experimental

The SiC ceramic in this study was prepared by pressureless sintering (supplied by Kaifa Special Ceramics Co., Ltd., Beijing, China). The CoFeCrNiCu alloy was

prepared by arc melting of pure elements, and then suction-casted into a rod with a diameter of 6 mm under an argon ambience. The SiC ceramics was cut into dimensions of 4 mm × 4 mm × 4 mm and 10 mm × 10 mm × 4 mm for metallographic observation and strength testing, respectively. The CoFeCrNiCu alloy was shaped to a foil with a thickness of 600 μm in an electrical discharge machine. The foil was grounded with the SiC grit paper until to a thickness of ~400 μm. All of the polished samples were ultrasonically cleaned in acetone for 10 min and then dried by an air flow.

Before brazing, the CoFeCrNiCu foil was intercalated in SiC ceramics, as shown in Fig. 1a. The assembly was then pinched by a graphite jig. A nominal load of 0.016 MPa was applied on the top to stabilize the assembly. During the brazing, a rate of 10 K/min was selected to heat up the assembly to 573 K. At this temperature, the assembly was held for 900 s to remove the binder. The brazing tests were performed in a vacuum brazing furnace (JVLF211) with a basic pressure less than 1.3×10^{-3} Pa. The brazing temperature was varied from 1433 K to 1473 K but the holding time fixed to 3600 s.

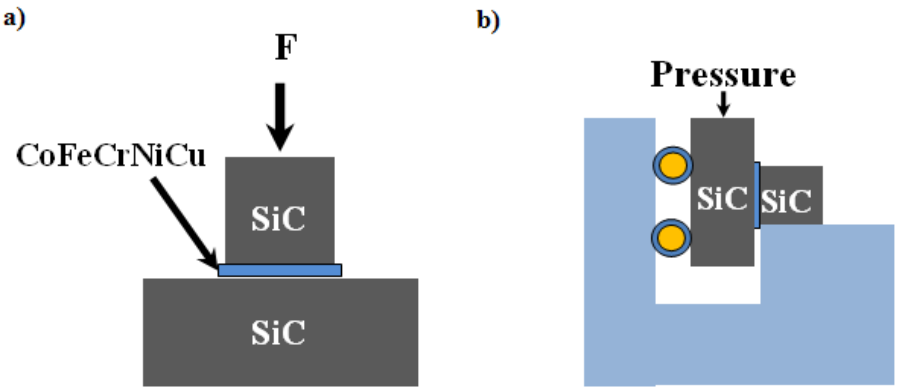

Fig. 1. Schematic diagram of a) brazing assembly and b) shear test.

The melting points of CoFeCrNiCu filler were analyzed by a differential thermal analysis (DTA, DTG-60H). The interfacial microstructure of the brazed joint was characterized on a scanning electron microscope (SEM, S-8010, Hitach, Japan) coupled with an energy dispersive spectrometer (EDS, TN-8000). The X-ray diffraction (XRD, D-MAX Rapid II) was utilized to identify the reaction phases of the brazed joint. To further investigate the micro-morphology and phase structures of the brazed joints, the seams were polished using a focused ion beam (FIB) method on a FEI Helios Nanolab 600 with the source material of Ga. The millings were performed with a voltage of 30 kV and 5 kV- 2 kV, for rough and fine millings. Source current was adjusted within a range of 90 pA - 22 nA during the FIB operation. The FIB samples were then analyzed via transmission electron microscopy (TEM) on a JEOL-2200FS EFTEM. To evaluate the mechanical property of the brazed joint, shear tests were carried out on a universal material testing machine (EUTM, MTS CMT4204) with a constant speed of 0.5 mm/min, as shown in Fig. 1b. At least three test results for a joint brazed at one temperature were used to calculate the average shear strength of the brazed joint.

3. Results and discussion

The microstructure of the CoCrCuFeNi alloy filler is depicted in Figs. 2(a) and (b). It is composed of a dendritic microstructure (darker phase α) and interdendrite microstructure (lighter phase β). The average primary arm width of the dendrites is about 15 μm. From the EDS results of Table 1, α is determined to the Cu-depleted phase (high-entropy FCC phase), and the Cu rich phase β to Cu(s, s). Hereafter, α phase is named as HEAF phase for convenience. Cu is reported as an electronegative element. It becomes less stable in the FCC dendrites and can be supplanted into the interdendritic regions and yielded Cu aggregations [22]. Combining XRD results of Fig. 2c, phases α and β are identified to Cu solid solutions but varied in Cu contents. The result is in line with these reported from Refs [20-23]. Fig. 2d demonstrates the DTA curve of CoCrCuFeNi filler. The liquid temperature T_l is about 1413 K. The brazing temperature set in the present work is higher than 1413 K.

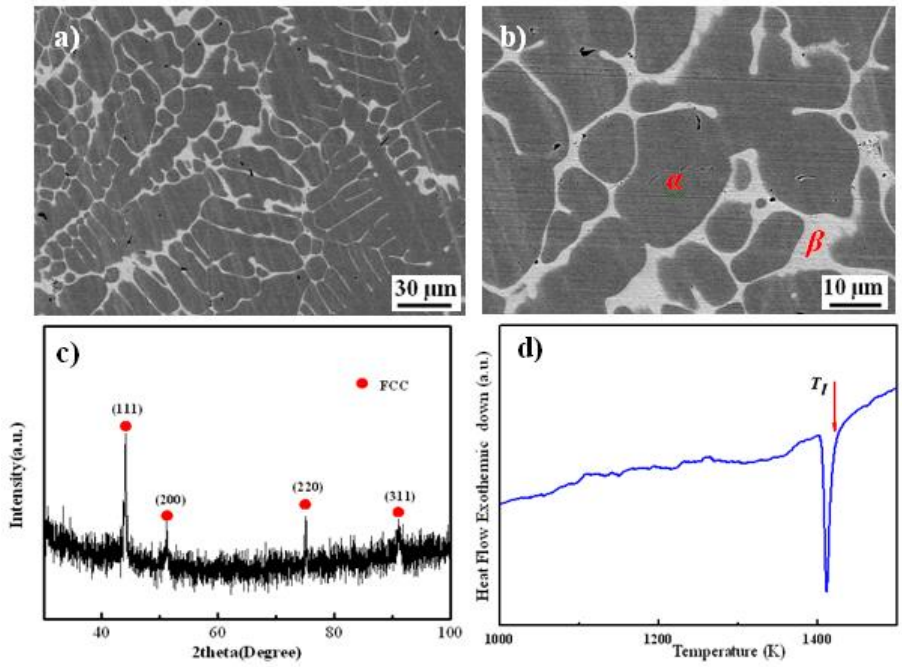

Fig. 2. a), b) microstructure; c) XRD pattern and d) DTA curve of CoCrFeNiCu alloy filler.

Table 1. EDS results from Fig. 2b.

Point	Co	Cr	Fe	Cu	Ni	phase
α	17.85	36.05	13.91	10.46	21.73	HEAF
β	12.77	14.41	11.51	50.58	10.73	Cu(s,s)

Figure 3 depicts the microstructure and EDS results of a SiC/CoFeCrNiCu/SiC joint brazed at 1453 K for 3600 s. A successful joint of SiC ceramics was reached. Obvious reaction layers appeared at the ceramic-metal interfaces as shown in Fig. 3a. Sufficient element distributions in the brazed joint can be well seen from Fig. 3b

to Fig. 3h. According to the distributions, the C, Si and Cr elements mainly locate at the reaction layer based on Figs. 3f-3h. The Co, Ni, Cu, Cr and Fe elements from the high entropy filler are mainly disorderly distributed in the whole brazing seam. Besides, it is worth noting that Cu from the high entropy alloy filler is distributed in the middle of joint, indicating the formation of Cu-based compound.

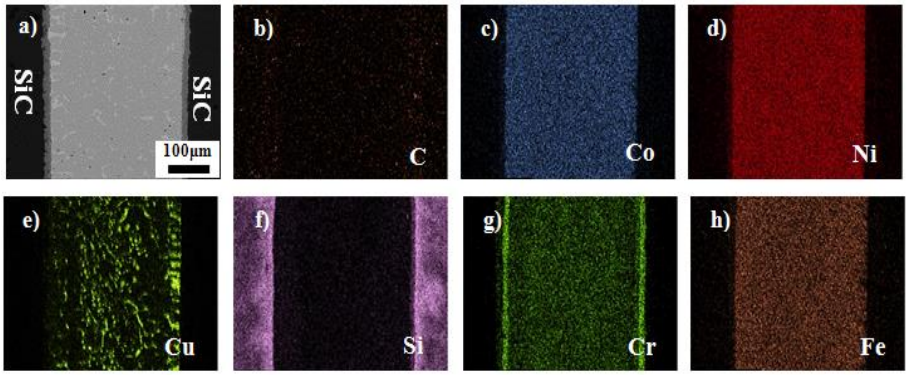

Fig. 3. a) Microstructure and b) to h) corresponding EDS results of brazed joint at 1453 K for 3600 s.

Figure 4a shows a typical microstructure of SiC/CoFeCrNiCu/SiC joint brazed at at 1453 K for 3600 s. In the overview, the joint is about 350 μm width without defects. A region of continuous reaction layers adjacent to SiC ceramic was found distinguishing from a region of the brazing seam. They were marked as zone I and zone II. Figs. 4b and 4c are the zoomed images of zones I and II. Zone I has an average width of ~15 μm. Therein three mixed phases are found, and marked as A, B and C. Zone II was the center zone of the joint with width of 300 μm where two phases were identified and marked as D and E.

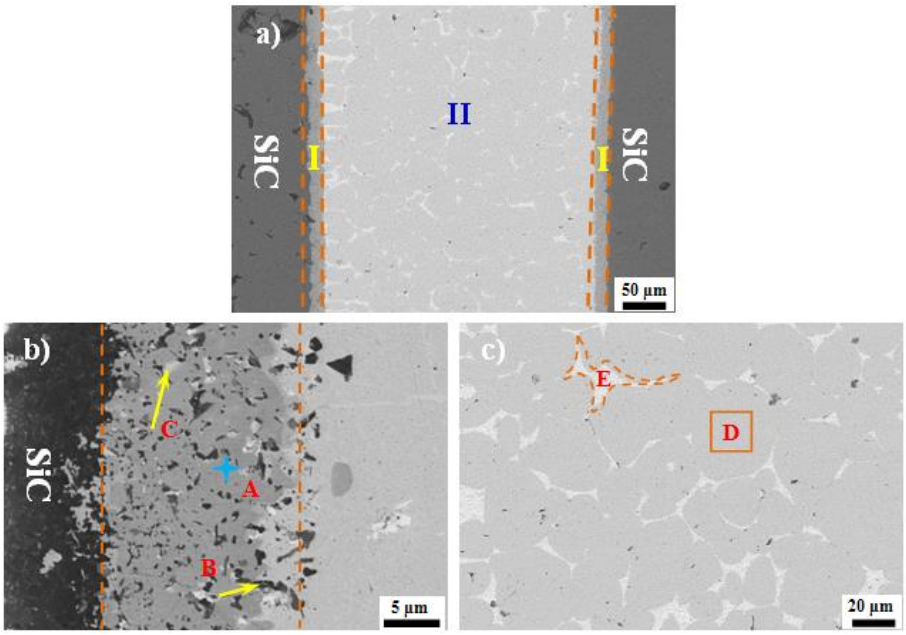

Fig. 4. SEM images of typical SiC/SiC brazed joint at 1453 K for 3600 s.

Chemical compositions of phases A-E in the brazed joint were tabulated in Table 2. The EDS determination identified the Cr and C in the gray phase A at a ratio of ~4:1. It is reported that for Cr, six compounds ($Cr_{23}C_6$, Cr_7C_3, Cr_3C_2, Cr_3Si, CrSi and Cr_5Si_3C) could be formed. Among them, the $Cr_{23}C_6$ phase is the most favorable because its formation requires lowest Gibbs free energy [24]. Combined the Cr and C ratio, phase A is inferred as $Cr_{23}C_6$. The main reaction between Cr and C underwent a process of $23Cr + 6C = Cr_{23}C_6$ (ΔG=-309600-77.4T (J/mol)). Such a Cr-C phase meets the necessary thermodynamic condition and can exist at a high temperature [25]. Moreover, high hardness and good oxidation resistance of $Cr_{23}C_6$ make it a reinforcing phase in the coating area. Thus, in the present work, the suitable formation of $Cr_{23}C_6$ phase can hinder the propagation of crack, and benefit strength of brazed joints [26, 27]. The main elements in the black phase B are Si, which is identified as the Si(s, s), consistent with the previous result where Cr-Si binary eutectic was

employed as a filler [28]. Phase C with tiny white structures mainly contains the Cu element. It is identified as Cu(s, s), corresponding to the previous research [29]. The molar ratio of Co, Cu, Cr, Ni and Fe in the gray phase D are about 1:1:1:1:1, while phase E is a cooper region. Thus, phases D and E are inferred as HEAF phase and Cu (s, s) phase, respectively. However, compared to results in Fig. 2a, the primary dendrites of as-cast filler alloy are significantly refined and form the equiaxed dendrite in the brazing seam. During brazing process, the solute contents are nearly equal for the Co, Cr, Fe and Ni elements in the high phase. In this context, a solute diffusion-controlled growth determines the dendritic velocity, and the HEAF phase grows in a dendritic path. On the other hand, a larger potential barrier inhibits the Cu solute during the solidification [30].

Table 2. EDS of each point marked in Fig. 4.

spot	C	Fe	Co	Ni	Cu	Si	Cr	Possible phase
A	14.41	1.60	0.89	1.06	6.13	4.04	71.87	$Cr_{23}C_6$
B	10.00	0.32	2.61	7.16	1.65	50.56	27.70	Si(s, s)
C	11.97	0.94	0.02	5.14	77.42	1.39	3.12	Cu(s, s)
D	13.09	11.75	15.55	18.29	11.23	2.56	27.53	FCC(HEAF)
E	11.39	0.96	0.01	5.03	79.15	0.65	2.81	Cu(s, s)

In order to reveal micro- and phase structures of the product in the joint, TEM and the selected area electron (SEAD) patterns of zone I and zone II were analyzed, as shown in Fig. 5. From Fig. 5a, main phases of $Cr_{23}C_6$, Cu(s,s) and Si(s,s) were well figured out. The corresponding SAED patterns were depicted in Figs. 5b and 5c for the crystals. Spots are identified as diffractions from the [3 4 7] and [1$\bar{1}$0] zone axis for Cu(s, s) and Si(s, s), respectively. Similarly, zone II are mainly Cu(s, s) and FCC HEAF phase, as shown in Fig. 5d. The strong diffraction spots are indexed to diffractions from [224] and [0$\bar{2}$2] zone axis for HEAF phase and Cu(s, s), respectively. Figure 6 demonstrates the micro-focused XRD pattern obtained from zone I and zone II, respectively. The XRD results are consistent with the analysis of SEM and TEM. From the above analysis, it can be determined that the A-E phases in the brazed joint are HEAF, Cu (s, s), Cu (s, s), Si(s, s), and $Cr_{23}C_6$, respectively.

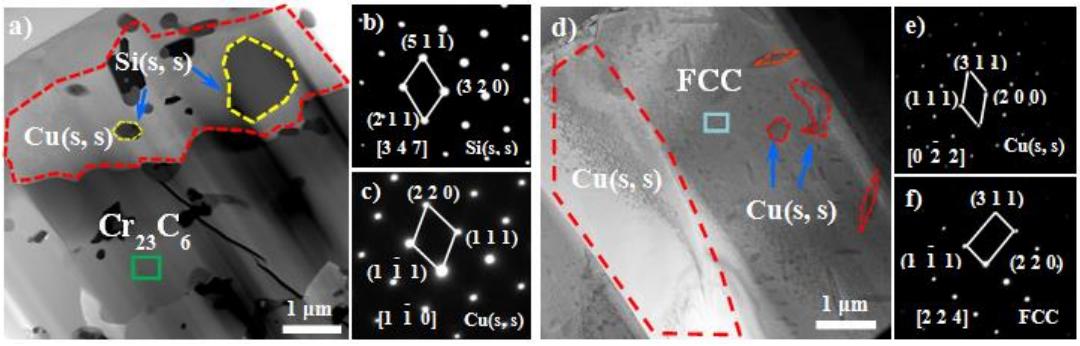

Fig. 5. TEM images and corresponding SAED patterns from: a)-c) zone I and d)-f) zone II.

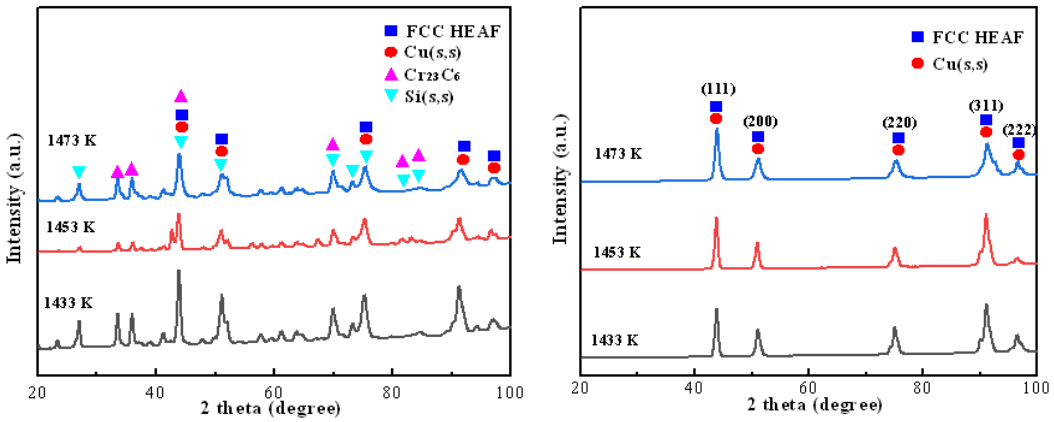

Fig. 6. Micro-focused XRD pattern of brazed joint at 1453 K for 3600 s from: a) zone I b) zone II.

The formation mechanism of the SiC/CoFeCrNiCu/SiC joint is systematically investigated. In Fig. 7, a physical model is established and the diagram of the brazed joint visualized. At the beginning, the CoFeCrNiCu filler was melt at the melting point of 1413 K based on the DTA result. During the heat process below 1413 K, the plastically deformed filler tightly contacted with ceramics, as shown in Fig. 7a. When the temperature reached above 1413K, the molten CoFeCrNiCu filler transformed into liquid and wetted the surface of the base materials. At the same time, partial base materials were dissolved into the molten alloy. The main elements of SiC and filler began to diffuse, as shown in Fig. 7b. When the temperature was elevated to the brazing temperature, SiC dissolved into the brazing alloy and released Si and C atoms. The active element of the Cr diffused to the SiC at both sides. Cr element is more active than other elements in CoFeCrNiCu alloy. The mixing enthalpies between Cu, and Fe, Co, Ni, C Cr are +12, -1, -4, -7 and -61 kJ/mol, respectively. However, the mixing enthalpies between Fe, Co, Ni and Cu are respectively + 13, + 6, and +4

kJ/mol [31]. Due to differences in enthalpies, Cr is capable to react with other elements, especially C. Energetically favorable reactions between the Cr and SiC happened. As a result, the $Cr_{23}C_6$ phases and Si phases were formed. Chemical reaction took place as $Cr + SiC \rightarrow Cr_{23}C_6 + Si$ [29, 32], as shown in Fig. 7c., The residual liquid brazing alloy was solidified into a solid solution during the cooling process following the high entropy effect. It further became the matrix of joints. In the last stage, zone I became thicker because of continued reactions between SiC and filler. However, due to the high entropy effect and slow diffusion effect of high entropy alloys, the center of the joint still held a high entropy alloy structure [33]. When the temperature decreased to the melting point of Cu, the Cu-enriched phase started to solidify from the liquid alloy [34]. As reported, mixing enthalpies between Fe, Cr, Co, Ni and Cu are respectively + 13, + 12, + 6, and +4 kJ/mol [35]. Thermodynamically, the Cu is not capable to react with other elements. Alternatively, weak mutual solubilities between Cu and the other elements lead to segregations of Cu rich phase in the joint, resulting in the formation of Cu(s, s), as shown in Fig. 7d. Following the further decrease of temperature, no other phase precipitated from the molten and the growth of the primary CoCrFeNiCu FCC solid solution phase continued. Due the diffusion of Cu element and the repulsion from other elements, some Cu was also pushed into reaction layer and formed Cu(s, s) in the interface, as shown in Fig. 7e. Based on the above analysis, it can be found that the Cr element can stabilize the Cu element in CoFeCrNiCu HEA due to the active of Cr, and reaction between Cr and SiC. Thus, in order to obtain a metallurgical bonding of joint when

using the HEA filler, the active element in the alloy is also necessary to initiate the interfacial reaction. This is a crucial factor to reconsider other HEA filler.

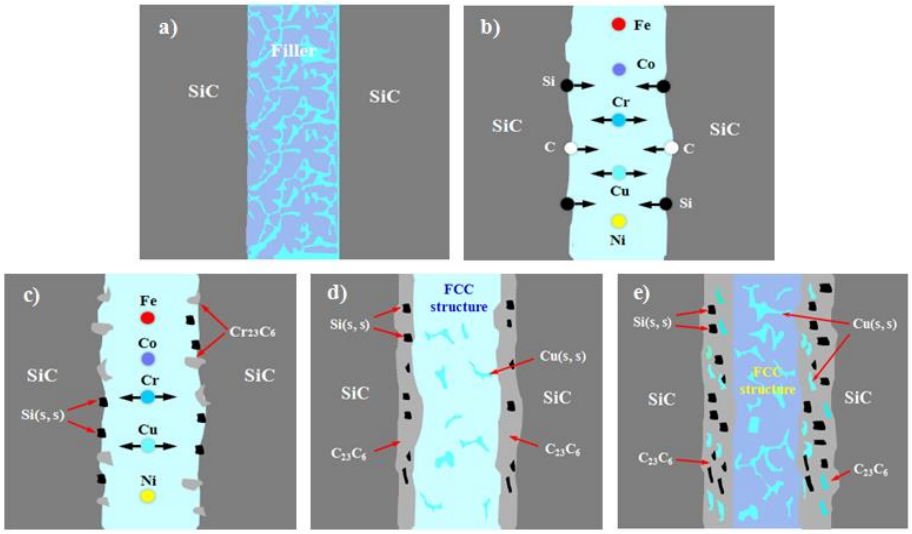

Fig. 7. Schematic diagram of microstructural evolution of SiC/SiC brazed joint

The shear strengths of SiC/SiC brazed joints brazed were plotted following brazing temperature changes at a fixed time of 3600 s, as shown in Fig. 8. All obtained joints own good shear strength despite temperature variations. At 1433 K, 1453 K and 1473 K, the shear strengths are 51 MPa, 60 MPa and 48 MPa, respectively. All values are higher than theses given by brazing with conventional Ag-Cu-Ti fillers [36]. Thus, it can be concluded that the activity of Cr is kept in the high entropy filler and ensures the interface reaction. At the same time, the FCC solid solutions, such as HEAF phase and Cu (s, s), form the matrix of the bulk of brazing seam. Generated by the mismatch of coefficients of thermal expansion between ceramic and metal, the residual stress is released thanks to this solid solution microstructure in the seam.

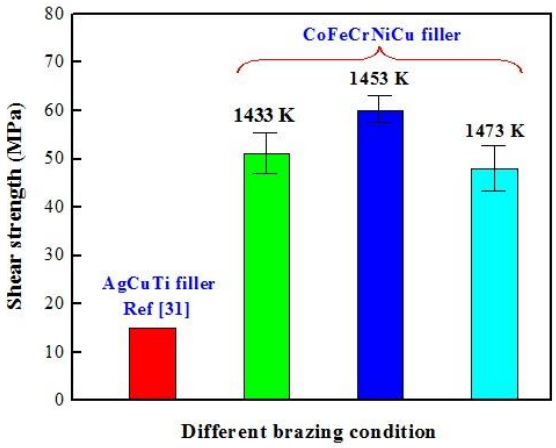

Fig. 8. The shear strength of SiC/SiC brazed joints brazed in the present and other works

Figure 9 depicts the microstructures of SiC joints brazed at different brazing temperatures. The brazing temperature affects the microstructure slightly. Similar to the case of 1453 K, two obviously zones were found in the resulted joints. Besides, there is no change in the phase type of the brazed joint, and the central region of the joint is an equiaxed dendritic high-entropy alloy solid solution structure, as shown in Figs. 9a, 9d and 9g. These claims are supported by the XRD results from Fig. 5. However, changes of micro-morphology appeared at individual zone following the temperature increase. In the middle of joints, Cu-rich spherical structures are observed in the brazed joint at a low temperature (1433 K). This indicates an occurrence of the liquid phase separation in the initial liquid prior to the liquid solid transformation. The Cu-rich droplets appeared firstly [37]. Relatively, the molten subjects surrounding the Cu-rich droplets contains copper depletion. As shown in Fig. 9c, typical equiaxed dendrite and interdendritic structures were yielded through the solidification. The former is rich in Co, Cr and Fe elements, and the latter in Cu and Ni elements. In the reaction layers on both sides of SiC, reaction layer increased from 10 μm to 20 μm

with the brazing temperature (Figs. 9b, 9f and 9h).

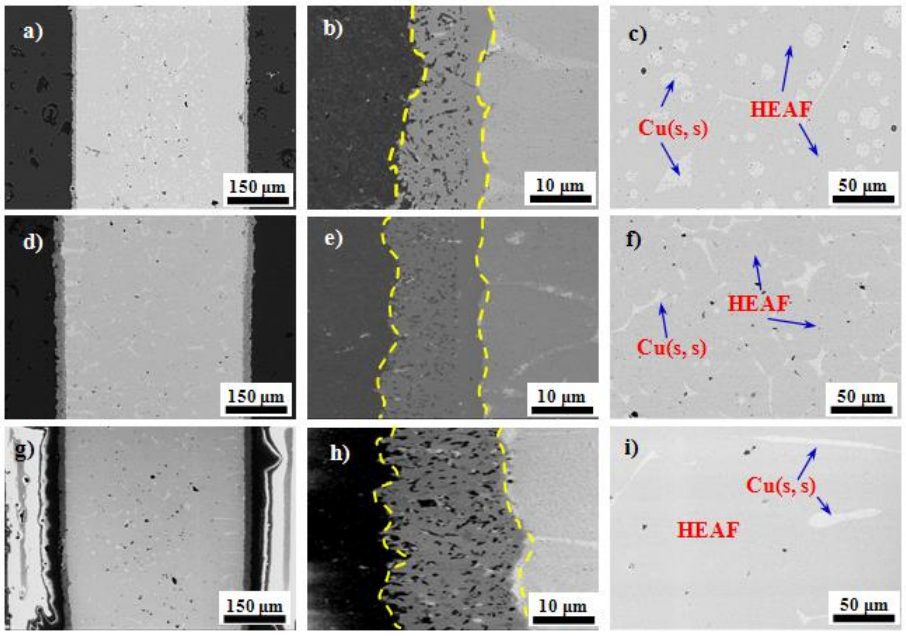

Fig. 9. Microstructures of SiC joints brazed at different brazing temperatures: a, b, c) 1433 K, d, e, f) 1453 K and g, h, i) 1473 K.

The formation path affects mechanical properties eventually. The shear strength was low when brazing temperature was below 1453 K as given by results of shear strength in Fig. 8. At these temperatures, atomic diffusions were low, and reactions remained insufficient between the filler alloy and the base materials. At brazing temperatures above 1453 K, the joint strength decreased. The interface became much thicker than before. Both mismatches of thermal expansion coefficients and Young's modulus resulted in large residual stresses between the alloyed filler and the ceramic. The joint is no more homogenous but containing micro-cracks [38, 39]. From the aforementioned determinations, the optimized condition of brazing is found as ~15 μm for the filler thickness and brazing at 1453 K for 3600 s.

Fig. 10 shows morphologies of the fracture surfaces of the SiC joint brazed at 1433 K to 1473 K for 3600 s, respectively. In brazing, the filler was well expanded, and reactions at interfaces were well accomplished, as shown in Figs. 10a to 10c. It is worth noting that a small amount of residual SiC ceramic was detected from the fracture surface from Fig. 10b. When the brazing temperature is 1433 K, as shown in Fig. 10d, two obvious different layers are formed. Consequentially, the stress concentration is easily induced and a weak joint yielded. When the brazing temperature is 1453 K, due to sufficient interface reaction and FCC solid solution in the brazing seam, the fracture takes place in the SiC ceramics substrate, as shown in Fig. 10e. When brazing was taken place at 1473 K, the Cr and C vigorously reacted. This leads to excessive Cr-C phase ($Cr_{23}C_6$) at the joint, inducing the formation of micro-cracks during brazing. Thus, during shear test, fracture can easily occur along these cracks, as shown in Fig. 10f.

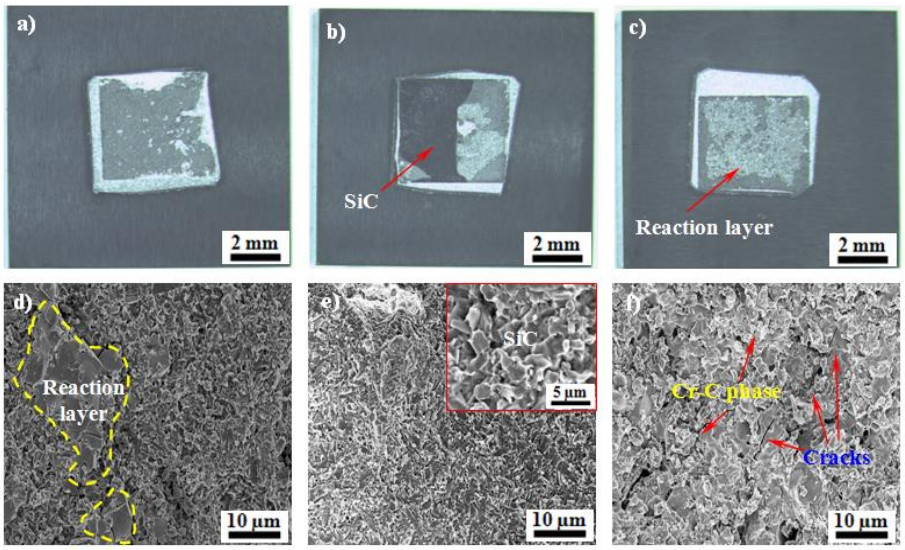

Fig. 10. Fracture surface of SiC/SiC brazed joint after shear test at different brazing temperature for 3600 s: a) and d) 1433 K; b) and e) 1453 K; c) and f) 1473 K.

4. Conclusion

In this present work, a novel CoFeCrNiCu high entropy alloy filler was prepared and introduced to braze SiC. Comprehensive properties of the brazed joints were investigated. The following are the main conclusions:

1) A sound joint was obtained at different brazing temperature for 3600 s using CoFeCrNiCu high entropy alloy filler. Due to the high entropy effect, the filler alloy is prone to form solid solution rather than intermetallic compounds. Variation of the brazing temperature brings slight changes for the microstructure of SiC joint. The typical microstructure of brazed joint is SiC/$Cr_{23}C_6$ + Cu(s, s) + Si(s, s)/HEAF + Cu(s, s)/ $Cr_{23}C_6$ + Cu(s, s) + Si(s, s)/SiC.

2) When using the high entropy filler, the brazed joints own higher shear strengths than these brazed with common AgCuTi filler, regardless the changes of brazing temperature. The maximum shear strength achieved 60 MPa at 1453 K for 3600 s. Higher or lower brazing temperature is not beneficial for the achieving of good joint quality.

3) A large quantity of FCC solid solution (e.g., HEAF phase and Cu (s, s)) was formed as the matrix of the bulk of brazing seam. It led to the release of the high residual stress of joint. At the same time, the suitable formation of $Cr_{23}C_6$ phase with high hardness can hinder the propagation of crack. Both factors benefit the strength of brazed joints.

4) During the formation of joint, the loss of Cr elements may indeed influence solid solution structure of original HEA. In the present work, with the increasing of

temperature, the solid solution structure in the seaming was changed. Such a question deserves inventions of composite fillers based on the HEA and a dedicated study in the future.

Acknowledgement

This work was financially supported by the National Natural Science Foundation of China [51704001, 51772028, 51772028]; Talent Project of Anhui Province [Z175050020001]; Natural Science Foundation of Anhui Province [KJ2018A0860], Talent Project of Anhui Polytechnic University, Anhui Provincial Grant for high-level platform construction, and the Academy of Finland [No. 311934], , and the Opening Project of State Key Laboratory of High Performance Ceramics and Superfine Microstructure [No.SKL201902SIC]. The Center of Microscopy and Nanotechnology of University of Oulu is also acknowledged for materials characterizations.

References

[1] M. Khodaei, O. yaghobizadeh, S. Hojat Naghavi Alhosseini, S. esmaeeli, S.R. Mousavi. The effect of oxide, carbide, nitride and boride additives on properties of pressureless sintered SiC: A review, J. Eur. Ceram. Soc. 39 (2019) 2215-2231. https://doi.org/10.1016/j.jeurceramsoc.2019.02.042.

[2] G. Liu, X. Zhang, J. Yang, G. Qiao, Recent advances in joining of SiC-based materials (monolithic SiC and SiCf/SiC composites): Joining processes, joint strength, and interfacial behavior, J. Adv. Ceram. 8 (2019) 19-38. https://xs.scihub.ltd/https://doi.org/10.1007/s40145-018-0297-x.

[3] X. Zhou, J. Liu, S. Zou, K. Xu, K. Chang, P. Li, F. Huang, Z. Huang, Q. Huang, Almost seamless joining of SiC using an in-situ reaction transition phase of

$Y_3Si_2C_2$, J. Eur. Ceram. Soc. 40 (2020) 259-266. https://doi.org/10.1016/j.jeurceramsoc.2019.10.016.

[4] N. Murayama, K. Hirao, M. Sando, T. Tsuchiya, H. Yamaguchi. High-temperature electro-ceramics and their application to SiC power modules, Ceram. Int. 44 (2018) 3523-3530. https://doi.org/10.1016/j.ceramint.2017.11.140.

[5] X. Lv, F. Ye, L. Cheng, S. Fan, Y. Liu, Fabrication of SiC whisker-reinforced SiC ceramic matrix composites based on 3D printing and chemical vapor infiltration technology, J. Eur. Ceram. Soc. 39 (2019) 3380-3386. https://doi.org/10.1016/j.jeurceramsoc.2019.04.043.

[6] R. Rakshit, A. Das, A review on cutting of industrial ceramic materials, Precis. Eng. 59 (2019) 90-109. https://doi.org/10.1016/j.precisioneng.2019.05.009.

[7] J. Li, L. Liu, Y. Wu, Z. Li, W. Zhang, W. Hu, Microstructure of high temperature Ti-based brazing alloys and wettability on SiC ceramic, Mater. Des. 30 (2009) 275-279. https://doi.org/10.1016/j.matdes.2008.04.070.

[8] P. Wan, M. Li, K. Xu, H.B. Wu, K.K. Chang, X.B. Zhou, X.D. Ding, Z.R. Huang, H.X. Zong, Q. Huang. Seamless joining of silicon carbide ceramics through an sacrificial interlayer of $Dy_3Si_2C_2$. J. Eur. Ceram. Soc. 39 (2019) 5457-5462. https://doi.org/10.1016/j.jeurceramsoc.2019.09.002.

[9] M. Li, X.B. Zhou, H. Yang, S.Y. Du, Q. Huang. The critical issues of SiC materials for future nuclear systems. Scripta Mater. 143 (2018) 149-153 https://doi.org/10.1016/j.scriptamat.2017.03.001.

[10] B. Chen, H. Xiong, Y. Cheng, W. Mao, S. Wu, Microstructure and property of AlN joint brazed with Au-Pd-Co-Ni-V brazing filler, J. Mater. Sci. Technol. 31 (2015) 1034-1038. https://doi.org/10.1016/j.jmst.2014.11.026.

[11] J. Yang, J. Huang, Z. Ye, S.H. Chen, R. Ji, Y. Zhao, Influence of interfacial reaction on reactive wettability of molten Ag-Cu-X wt. %Ti filler metal on SiC ceramic substrate and mechanism analysis, Appl. Surf. Sci. 436 (2018) 768-778. https://doi.org/10.1016/j.apsusc.2017.12.106.

[12] Q. Qi, J. Zhang, H. Hu, Benefits of Zr additive element in the Ti-24Ni eutectic filler in vacuum brazing of SiC ceramics, Vaccum. 162 (2019) 110-113. https://doi.org/10.1016/j.vacuum.2019.01.034.

[13] X. Dai, J. Cao, Z. Chen, X. Song, J. Feng, Brazing SiC ceramic using novel B_4C reinforced Ag-Cu-Ti composite filler, Ceram. Int. 42 (2016) 6319-6328. https://doi.org/10.1016/j.ceramint.2016.01.021.

[14] Z. Zhong, G. Hou, Z. Zhu, Z. Wang, G. Wang, Y. Wu, Microstructure and mechanical strength of SiC joints brazed with Cr_3C_2 particulate reinforced Ag-Cu-Ti brazing alloy, Ceram. Int. 44 (2018) 11862-11868. https://doi.org/10.1016/j.ceramint.2018.04.002.

[15] W. Zhang, P. Liaw, Y. Zhang, Science and technology in high-entropy alloys, Sci. China. Mater. 61 (2018) 2-22. https://xs.scihub.ltd/https://doi.org/10.1007/s40843-017-9195-8.

[16] W. Ji, W. Wang, H. Wang, J. Zhang, Y. Wang, F. Zhang, Z. Fu, Alloying behaviour and novel properties of CoCrFeNiMn high-entropy alloy fabricated by mechanical alloying and spark plasma sintering, Intermetallics. 56 (2015) 24-27. https://doi.org/10.1016/j.intermet.2014.08.008.

[17] N. Nayan, G. Singh, S.V.S.N. Murty, A. Jha, B. Pant, K. George, U. Ramamurty, Hot deformation behaviour and microstructure control in AlCrCuNiFeCo high entropy alloy, Intermetallics. 55 (2014) 145-153. https://doi.org/10.1016/j.intermet.2014.07.019.

[18] L. Zhang, J. Shi, H. Li, Interfacial microstructure and mechanical properties of ZrB_2-SiC-C ceramic and GH99 superalloy joints brazed with a Ti-modified FeCoNiCrCu high-entropy alloy, Mater. Des. 97 (2016) 230-238. https://doi.org/10.1016/j.matdes.2016.02.055.

[19] D. Bridges, S. Zhang, S. Lang, M. Gao, Z. Yu, Z. Feng, A. Hu, Laser brazing of a nickel-based superalloy using a Ni-Mn-Fe-Co-Cu high entropy alloy filler metal, Mater. Lett. 215 (2018) 11-14. https://doi.org/10.1016/j.matlet.2017.12.003.

[20] X. Wang, Y. Zhang, Y. Qiao, Novel microstructure and properties of multi-component $CoCrCuFeNiTi_x$ alloys, Intermetallics. 15 (2007) 357-362. https://doi.org/10.1016/j.intermet.2006.08.005.

[21] B. Wu, Z.Y. Xie, J.C. Huang, et al. Microstructures and thermodynamic properties of high-entropy alloys CoCrCuFeNi. Intermetallics 93 (2018) 40-46. https://doi.org/10.1016/j.intermet.2017.10.018

[22] H. Cui, L. Zheng, J. Wang, Microstructure evolution and corrosion behavior of directionally solidified FeCoNiCrCu high entropy alloy, Appl. Mech. Mater. 66-68 (2011) 146-149. https://doi.org/10.4028/www.scientific.net/AMM.66-68.146.

[23] Y. Hsu, W. Chiang, J. Wu, Corrosion behavior of FeCoNiCrCux high-entropy alloys in 3.5% sodium chloride solution, Mater. Chem. Phys. 92 (2005) 112-117. https://doi.org/10.1016/j.matchemphys.2005.01.001.

[24] G. Liu, M. Muolo, F. Valenza, A. Passerone, Survey on wetting of SiC by molten metals, Ceram. Int. 36 (2010) 1177-1188. https://doi.org/10.1016/j.ceramint.2010.01.001.

[25] F. Ye, M. Hojamberdiev, Y. Xu, L. Zhong, H. Yan, Z. Chen, $(Cr, Fe)_7C_3$/Fe surface gradient composite: Microstructure, microhardness, and wear resistance, Mater. Chem. Phys. 147 (2014) 823-830. https://doi.org/10.1016/j.matchemphys.2014.06.026.

[26] Y. Liu, J. Han, R. Li, W. Li, X. Xu, J. Wang, X. Xu, J. Wang, S. Yang, Microstructure and dry-sliding wear resistance of PTA clad $(Cr, Fe)_7C_3$/γ-Fe ceramal composite coating, Appl. Surf. Sci. 252 (2006) 7539-7544. https://doi.org/10.1016/j.apsusc.2005.09.008.

[27] G. Wang, Y. Cai, W. Wang, K. Gui, D. Zhu, C. Tan, W. Cao, Brazing ZrB_2-SiC ceramics to Inconel 600 alloy without and with Cu foam, J. Manuf. Process. 41 (2019) 29-35. https://doi.org/10.1016/j.jmapro.2019.03.023.

[28] H. Li, Z. Wang, Z. Zhong, Q. Wen, K. Song, H. Zhang, Y. Wu, Micro-alloying effects of yttrium on the microstructure and strength of silicon carbide joint

brazed with chromium-silicon eutectic alloy, J. Alloys Compd. 738 (2018) 354-362. https://doi.org/10.1016/j.jallcom.2017.12.137.

[29] Z. Zhu, K. Ma, Q. Wang, C. Shek, Compositional dependence of phase formation and mechanical properties in three CoCrFeNi-(Mn/Al/Cu) high entropy alloys, Intermetallics. 79 (2016) 1-11. https://doi.org/10.1016/j.intermet.2016.09.003.

[30] W. Wang, L. Hu, S. Luo, L. Meng, D. Geng, B. Wei, Liquid phase separation and rapid dendritic growth of high-entropy CoCrCuFeNi alloy, Intermetallics. 77 (2016) 41-45. https://doi.org/10.1016/j.intermet.2016.07.003.

[31] A. Takeuchi, A. Inoue. Classification of bulk metallic glasses by atomic size difference, heat of mixing and period of constituent elements and its application to characterization of the main alloying element. Mater. Trans 46(12) (2005) 2817-2829.https://doi.org/10.2320/matertrans.46.2817

[32] S. Yang, N. Li, H. Li, Effects of electric pulse treatment on shape memory effect and microstructure in a pre-deformation $Fe_{13}Mn_6Si_{13}Cr_4Ni_{0.1}C$ alloy, Rare. Metal. Mater. Eng. 45(1) (2016) 51-55. https://doi.org/10.1016/S1875-5372(16)30045-5.

[33] R. Wang, W. Chen, J. Zhong, L. Zhang, Experimental and numerical studies on the sluggish diffusion in face centered cubic Co-Cr-Cu-Fe-Ni high-entropy alloys, J. Mater. Sci. Technol. 34 (2018) 1791-1798. https://doi.org/10.1016/j.jmst.2018.02.003.

[34] H. Zheng, R. Chen, G. Qin, X. Li, Y. Su, H. Ding, J. Guo, H. Fu, Microstructure evolution, Cu segregation and tensile properties of CoCrFeNiCu high entropy alloy during directional solidification, Mater. Sci. Technol. 38 (2020) 19-27. https://doi.org/10.1016/j.jmst.2019.08.019.

[35] A. Takeuchi, A. Inoue, Calculations of amorphous-forming composition range for ternary alloy systems and analyses of stabilization of amorphous phase and amorphous-forming ability, Mater. Trans. Jim. 42 (2001) 1435-1444. https://doi.org/10.2320/matertrans.42.1435.

[36] Y. Song, D. Liu, S. Hu, X. Song, J. Cao, Graphene nanoplatelets reinforced AgCuTi composite filler for brazing SiC ceramic, J. Eur. Ceram Soc. 39 (2019) 696-704. https://doi.org/10.1016/j.jeurceramsoc.2018.11.046.

[37] P. Wu, N. Liu, P. Zhou, Z. Peng, W. Du, X. Wang, Y. Pan, Microstructures and liquid phase separation in multi-component CoCrCuFeNi high entropy alloys, Mate. Sci. Technol. 32(6) (2016) 576-580. https://doi.org/10.1179/1743284715Y.0000000127.

[38] G. Wang, Y. Yang, P. Wu, D. Shu, D. Zhu, C. Tan, W. Cao, Effect of brazing temperature on microstructure and mechanical properties of TiAl/ZrB_2 joint brazed with CuTiZrNi filler, J. Manuf. Process. 46 (2019) 170-176. https://doi.org/10.1016/j.jmapro.2019.09.001.

[39] X. Tian, J. Feng, J. Shi, H. Li, L. Zhang, Brazing of ZrB_2-SiC-C ceramic and GH_{99} superalloy to form reticular seam with low residual stress, Ceram. Int. 41 (2015) 145-153. https://doi.org/10.1016/j.ceramint.2014.08.051.

Figure Captions

Fig. 1. Schematic diagram of a) brazing assembly and b) shear test.

Fig. 2. a), b) microstructure; c) XRD pattern and d) DTA curve of CoCrFeNiCu alloy filler.

Fig. 3. a) Microstructure and b) to h) corresponding EDS results of brazed joint at 1453 K for 3600 s.

Fig. 4. SEM images of typical SiC/SiC brazed joint at 1453 K for 3600 s.

Fig. 5. TEM images and corresponding SAED patterns from: a)-c) zone I and d)-f) zone II.

Fig. 6. Micro-focused XRD pattern of brazed joint at 1453 K for 3600 s from: a) zone I b) zone II.

Fig. 7. Schematic diagram of microstructural evolution of SiC/SiC brazed joint.

Fig. 8. The shear strength of SiC/SiC brazed joints brazed in the present and other works.

Fig. 9. Microstructures of SiC joints brazed at different brazing temperatures: a, b, c) 1433 K, d, e, f) 1453 K and g, h, i) 1473 K.

Fig. 10. Fracture surface of SiC/SiC brazed joint after shear test at different brazing temperature for 3600 s: a) and d) 1433 K; b) and e) 1453 K; c) and f) 1473 K.

Table Captions

Table 1. EDS results from Fig. 2b.

Table 2. EDS of each point marked in Fig. 4.